

Geometric Understanding of Deep Learning

Na Lei ^{*} Zhongxuan Luo [†] Shing-Tung Yau [‡] David Xianfeng Gu [§]

Abstract

Deep learning is the mainstream technique for many machine learning tasks, including image recognition, machine translation, speech recognition, and so on. It has outperformed conventional methods in various fields and achieved great successes. Unfortunately, the understanding on how it works remains unclear. It has the central importance to lay down the theoretic foundation for deep learning.

In this work, we give a geometric view to understand deep learning: we show that the fundamental principle attributing to the success is the manifold structure in data, namely natural high dimensional data concentrates close to a low-dimensional manifold, deep learning learns the manifold and the probability distribution on it.

We further introduce the concepts of rectified linear complexity for deep neural network measuring its learning capability, rectified linear complexity of an embedding manifold describing the difficulty to be learned. Then we show for any deep neural network with fixed architecture, there exists a manifold that cannot be learned by the network. Finally, we propose to apply optimal mass transportation theory to control the probability distribution in the latent space.

arXiv:1805.10451v2 [cs.LG] 31 May 2018

^{*}Dalian University of Technology, Dalian, China. Email: nalei@dlut.edu.cn

[†]Dalian University of Technology, Dalian, China. Email: zxluo@dlut.edu.cn

[‡]Harvard University, Boston, US. Email: yau@math.harvard.edu

[§]Harvard University, Boston, US. Email: gu@cmsa.fas.harvard.edu.

1 Introduction

Deep learning is the mainstream technique for many machine learning tasks, including image recognition, machine translation, speech recognition, and so on [12]. It has outperformed conventional methods in various fields and achieved great successes. Unfortunately, the understanding on how it works remains unclear. It has the central importance to lay down the theoretic foundation for deep learning.

We believe that the main fundamental principle to explain the success of deep learning is the **manifold structure** in the data, there exists a well accepted manifold assumption: *natural high dimensional data concentrates close to a non-linear low-dimensional manifold.*

Manifold Representation The main focus of various deep learn methods is to learn the manifold structure from the real data and obtain a parametric representation of the manifold. In general, there is a probability distribution μ in the ambient space \mathcal{X} , the support of μ is a low dimensional manifold $\Sigma \subset \mathcal{X}$. For example, an autoencoder learns the encoding map $\varphi_\theta : \mathcal{X} \rightarrow \mathcal{F}$ and the decoding map $\psi_\theta : \mathcal{F} \rightarrow \mathcal{X}$, where \mathcal{F} is the latent space. The parametric representation of the input manifold Σ is given by the decoding map ψ_θ . The reconstructed manifold $\tilde{\Sigma} = \psi_\theta \circ \varphi_\theta(\Sigma)$ approximates input manifold. Furthermore, the DNN also learns and controls the distribution induced by the encoder $(\varphi_\theta)_*\mu$ defined on the latent space. Once the parametric manifold structure is obtained, it can be applied for various application, such as randomly generating a sample on $\tilde{\Sigma}$ as a generative model. Image denoising can be reinterpreted geometrically as projecting a noisy sample onto $\tilde{\Sigma}$ representing the clean image manifold, the closest point on $\tilde{\Sigma}$ gives the denoised image.

Learning Capability An autoencoder implemented by a ReLU DNN offers a piecewise functional space, the manifold structure can be learned by optimizing special loss functions. We introduce the concept of *Rectified Linear Complexity* of a DNN, which represents the upper bound of the number of pieces of all the functions representable by the DNN, and gives a measurement for the learning capability of the DNN. On the other hand, the piecewise linear encoding map φ_θ defined on the ambient space is required to be homomorphic from Σ to a domain on \mathcal{F} . This requirement induces strong topological constraints of the input manifold Σ . We introduce another concept *Rectified linear Complexity* of an embedded manifold (Σ, \mathcal{X}) , which describes the minimal number of pieces for a PL encoding map, and measures the difficulty to be encoded by a DNN. By comparing the complexities of the DNN and the manifold, we can verify if the DNN can learn the manifold in principle. Furthermore, we show for any DNN with fixed architecture, there exists an embedding manifold that can not be encoded by the DNN.

Latent Probability Distribution Control The distribution $(\varphi_\theta)_*\mu$ induced by the encoding map can be controlled by designing special loss functions to modify the encoding map φ_θ . We also propose to use optimal mass transportation theory to find the optimal transportation map defined on the latent space, which transforms simple distributions, such as Gaussian or uniform, to $(\varphi_\theta)_*\mu$. Comparing to the conventional WGAN model, this method replaces the blackbox by explicit mathematical construction, and avoids the competition between the generator and the discriminator.

1.1 Contributions

This work proposes a geometric framework to understand autoencoder and general deep neural networks and explains the main theoretic reason for the great success of deep learning - the manifold structure hidden in data. The work introduces the concept of rectified linear complexity of a ReLU DNN to measure the learning capability, and rectified linear complexity of an embedded manifold to describe the encoding difficulty. By applying the concept of complexities, it is shown that for any DNN with fixed architecture, there is a

manifold too complicated to be encoded by the DNN. Finally, the work proposes to apply optimal mass transportation map to control the distribution on the latent space.

1.2 Organization

The current work is organized in the following way: section 2 briefly reviews the literature of autoencoders; section 3 explains the manifold representation; section 4 quantifies the learning capability of a DNN and the learning difficulty for a manifold; section 5 proposes to control the probability measure induced by the encoder using optimal mass transportation theory. Experimental results are demonstrated in the appendix 6.

2 Previous Works

The literature of autoencoders is vast, in the following we only briefly review the most related ones as representatives.

Traditional Autoencoders (AE) The *traditional autoencoder (AE)* framework first appeared in [2], which was initially proposed to achieve dimensionality reduction. [2] use linear autoencoder to compare with PCA. With the same purpose, [14] proposed a *deep autoencoder* architecture, where the encoder and the decoder are multi-layer deep networks. Due to non-convexity of deep networks, they are easy to converge to poor local optima with random initialized weights. To solve this problem, [14] used restricted Boltzmann machines (RBMs) to pre-train the model layer by layer before fine-tuning. Later [4] used traditional AEs to pre-train each layer and got similar results.

Sparse Encoders The traditional AE uses bottleneck structure, the width of the middle later is less than that of the input layer. The *sparse autoencoder (SAE)* was introduced in [10], which uses over-complete latent space, that is the middle layer is wider than the input layer. Sparse autoencoders [19, 21, 20] were proposed.

Extra regularizations for sparsity was added in the object function, such as the KL divergence between the bottle neck layer output distribution and the desired distribution [18]. SAEs are used in a lot of classification tasks [31, 26], and feature tranfer learning [8].

Denosing Autoencoder (DAE) [30, 29] proposed *denoising autoencoder (DAE)* in order to improve the robustness from the corrupted input. DAEs add regularizations on inputs to reconstruct a “repaired” input from a corrupted version. *Stacked denoising autoencoders (SDAEs)* is constructed by stacking multiple layers of DAEs, where each layer is pre-trained by DAEs. The DAE/SDAE is suitable for denosing purposes, such as speech recognition [9, 9], and removing musics from speeches [33], medical image denoising [11] and super-resolutions [7].

Contractive Autoencoders (CAEs) [24] proposed *contractive autoencoders (CAEs)* to achieve robustness by minimizing the first order variation, the Jacobian. The concept of contraction ratio is introduced, which is similar to the Lipschitz constants. In order to learn the low-dimensional structure of the input data, the panely of construction error encourages the contraction ratios on the tangential directions of the manifold to be close to 1, and on the orthogonal directions to the manifold close to 0. Their experiments showed that the learned representations performed as good as DAEs on classification problems and showed that their contraction properties are similar. Following this work, [23] proposed *the higher-order CAE* which adds an additional penalty on all higher derivatives.

Generative Model Autoencoders can be transformed into a generative model by sampling in the latent space and then decode the samples to obtain new data. [30] used Bernoulli sampling to AEs and DAEs to first implement this idea. [5] used Gibbs sampling to alternatively sample between the input space and the latent space, and transferred DAEs into generative models. They also proved that the generated distribution is consistent with the distribution of the dataset. [22] proposed a generative model by sampling from CADs. They used the information of the Jacobian to sample around the latent space.

The *Variational autoencoder (VAE)* [15] use probability perspective to interpret autoencoders. Suppose the real data distribution is μ in \mathcal{X} , the encoding map $\varphi_\theta : \mathcal{X} \rightarrow \mathcal{F}$ pushes μ forward to a distribution in the latent space $(\varphi_\theta)_*\mu$. VAE optimizes φ_θ , such that $(\varphi_\theta)_*\mu$ is normal distributed $(\varphi_\theta)_*\mu \sim \mathcal{N}(0, 1)$ in the latent space.

Followed by the big success of GANs, [17] proposed *adversarial autoencoders (AAEs)*, which use GANs to minimize the discrepancy between the push forward distribution $(\varphi_\theta)_*\mu$ and the desired distribution in the latent space.

3 Manifold Structure

Deep learning is the mainstream technique for many machine learning tasks, including image recognition, machine translation, speech recognition, and so on [12]. It has outperformed conventional methods in various fields and achieved great successes. Unfortunately, the understanding on how it works remains unclear. It has the central importance to lay down the theoretic foundation for deep learning.

We believe that the main fundamental principle to explain the success of deep learning is the manifold structure in the data, namely *natural high dimensional data concentrates close to a non-linear low-dimensional manifold*.

The goal of deep learning is to learn the manifold structure in data and the probability distribution associated with the manifold.

3.1 Concepts and Notations

The concepts related to manifold are from differential geometry, and have been translated to the machine learning language.

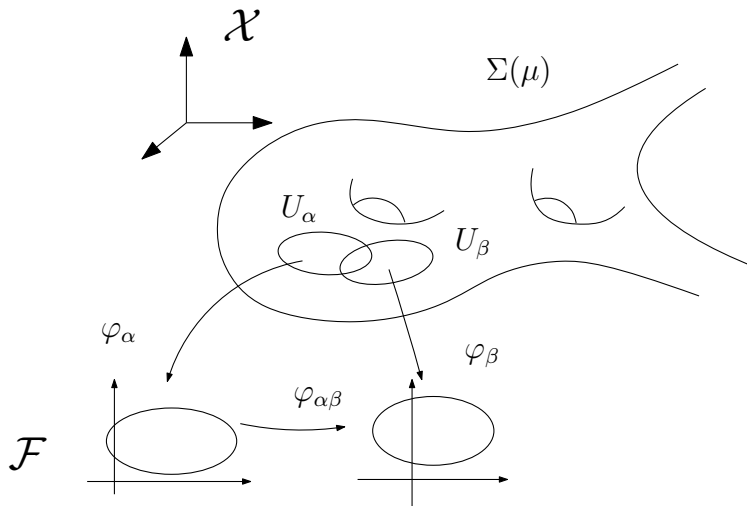


Figure 1: A manifold structure in the data.

Definition 3.1 (Manifold). An n -dimensional manifold Σ is a topological space, covered by a set of open sets $\Sigma \subset \bigcup_{\alpha} U_{\alpha}$. For each open set U_{α} , there is a homeomorphism $\varphi_{\alpha} : U_{\alpha} \rightarrow \mathbb{R}^n$, the pair $(U_{\alpha}, \varphi_{\alpha})$ form a chart. The union of charts form an atlas $\mathcal{A} = \{(U_{\alpha}, \varphi_{\alpha})\}$. If $U_{\alpha} \cap U_{\beta} \neq \emptyset$, then the chart transition map is given by $\varphi_{\alpha\beta} : \varphi_{\alpha}(U_{\alpha} \cap U_{\beta}) \rightarrow \varphi_{\beta}(U_{\alpha} \cap U_{\beta})$,

$$\varphi_{\alpha\beta} := \varphi_{\beta} \circ \varphi_{\alpha}^{-1}.$$

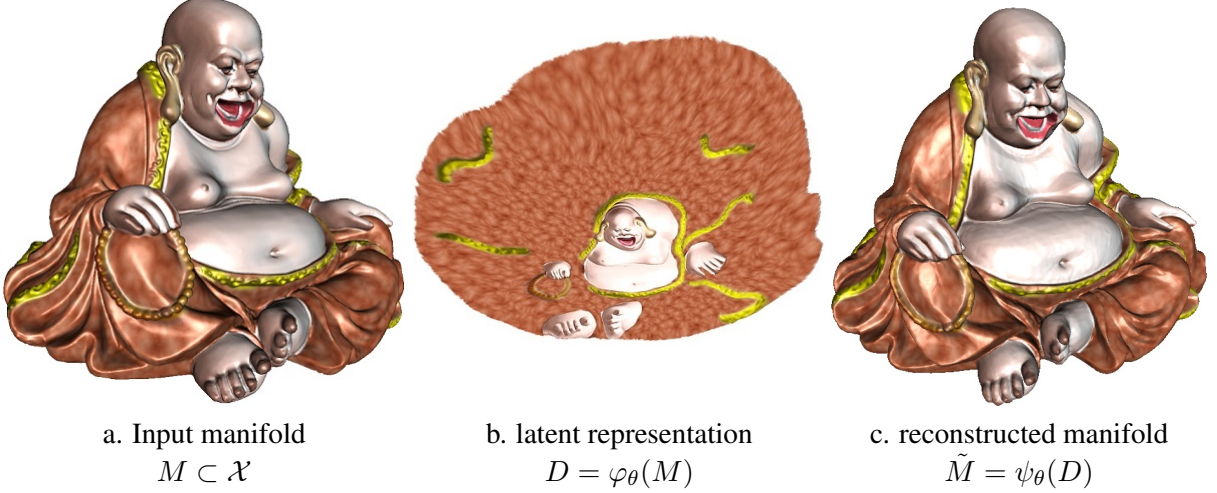


Figure 2: Auto-encoder pipeline.

As shown in Fig. 1, suppose \mathcal{X} is the *ambient space*, μ is a probability distribution defined on \mathcal{X} , represented as a density function $\mu : \mathcal{X} \rightarrow \mathbb{R}_{\geq 0}$. The *support* of μ ,

$$\Sigma(\mu) := \{\mathbf{x} \in \mathcal{X} | \mu(x) > 0\}$$

is a low-dimensional manifold. $(U_{\alpha}, \varphi_{\alpha})$ is a local chart, $\varphi_{\alpha} : U_{\alpha} \rightarrow \mathcal{F}$ is called an *encoding map*, the parameter domain \mathcal{F} is called the *latent space* or *feature space*. A point $\mathbf{x} \in \Sigma$ is called a *sample*, its parameter $\varphi_{\alpha}(\mathbf{x})$ is called the *code* or *feature* of \mathbf{x} . The inverse map $\psi_{\alpha} := \varphi_{\alpha}^{-1} : \mathcal{F} \rightarrow \Sigma$ is called the *decoding map*. Locally, $\psi_{\alpha} : \mathcal{F} \rightarrow \Sigma$ gives a local *parametric representation* of the manifold.

Furthermore, the encoding map $\varphi_{\alpha} : U_{\alpha} \rightarrow \mathcal{F}$ induces a *push-forward* probability measure $(\varphi_{\alpha})_*\mu$ defined on the latent space \mathcal{F} : for any measurable set $B \subset \mathcal{F}$,

$$(\varphi_{\alpha})_*\mu(B) := \mu(\varphi_{\alpha}(B)).$$

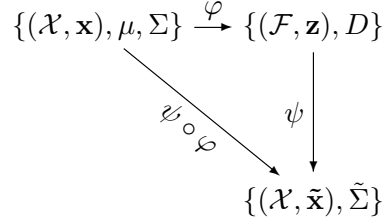
The goal for deep learning is to learn the encoding map φ_{α} , decoding map ψ_{α} , the parametric representation of the manifold $\psi_{\alpha} : \mathcal{F} \rightarrow \Sigma$, furthermore the push-forward probability $(\varphi_{\alpha})_*\mu$ and so on. In the following, we explain how an autoencoder learns the manifold and the distribution.

3.2 Manifold Learned by an Autoencoder

Autoencoders are commonly used for unsupervised learning [3], they have been applied for compression, denoising, pre-training and so on. In abstract level, autoencoder learns the low-dimensional structure of data and represent it as a parametric polyhedral manifold, namely a piecewise linear (PL) map from latent space (parameter domain) to the ambient space, the image of the PL mapping is a manifold. Then autoencoder utilizes the polyhedral manifold as the approximation of the manifold in data for various applications. In

implementation level, an autoencoder partition the manifold into pieces (by decomposing the ambient space into cells) and approximate each piece by a hyperplane as shown in Fig. 2.

Architecturally, an autoencoder is a feedforward, non-recurrent neural network with the output layer having the same number of nodes as the input layer, and with the purpose of reconstructing its own inputs. In general, a bottleneck layer is added for the purpose of dimensionality reduction. The input space \mathcal{X} is the ambient space, the output space is also the ambient space. The output space of the bottle neck layer \mathcal{F} is the latent space.



An autoencoder always consists of two parts, the encoder and the decoder. The encoder takes a sample $\mathbf{x} \in \mathcal{X}$ and maps it to $\mathbf{z} \in \mathcal{F}$, $\mathbf{z} = \varphi(\mathbf{x})$, the image \mathbf{z} is usually referred to as *latent representation* of \mathbf{x} . The encoder $\varphi : \mathcal{X} \rightarrow \mathcal{F}$ maps Σ to its latent representation $D = \varphi(\Sigma)$ homomorphically. After that, the decoder $\psi : \mathcal{F} \rightarrow \mathcal{X}$ maps \mathbf{z} to the reconstruction $\tilde{\mathbf{x}}$ of the same shape as \mathbf{x} , $\tilde{\mathbf{x}} = \psi(\mathbf{z}) = \psi \circ \varphi(\mathbf{x})$. Autoencoders are also trained to minimise reconstruction errors:

$$\varphi, \psi = \operatorname{argmin}_{\varphi, \psi} \int_{\mathcal{X}} \mathcal{L}(\mathbf{x}, \psi \circ \varphi(\mathbf{x})) d\mu(\mathbf{x}),$$

where $\mathcal{L}(\cdot, \cdot)$ is the loss function, such as squared errors. The reconstructed manifold $\tilde{\Sigma} = \psi \circ \varphi(\Sigma)$ is used as an approximation of Σ .

In practice, both encoder and decoder are implemented as ReLU DNNs, parameterized by θ . Let $X = \{\mathbf{x}^{(1)}, \mathbf{x}^{(2)}, \dots, \mathbf{x}^{(k)}\}$ be the training data set, $X \subset \Sigma$, the autoencoder optimizes the following loss function:

$$\min_{\theta} \mathcal{L}(\theta) = \min_{\theta} \frac{1}{k} \sum_{i=1}^k \|\mathbf{x}^{(i)} - \psi_{\theta} \circ \varphi_{\theta}(\mathbf{x}^{(i)})\|^2.$$

Both the encoder φ_{θ} and the decoder ψ_{θ} are piecewise linear mappings. The encoder φ_{θ} induces a cell decomposition $\mathcal{D}(\varphi_{\theta})$ of the ambient space

$$\mathcal{D}(\varphi_{\theta}) : \mathcal{X} = \bigcup_{\alpha} U_{\theta}^{\alpha},$$

where U_{θ}^{α} is a convex polyhedron, the restriction of φ_{θ} on it is an affine map. Similarly, the piecewise linear map $\psi_{\theta} \circ \varphi_{\theta}$ induces a polyhedral cell decomposition $\mathcal{D}(\psi_{\theta} \circ \varphi_{\theta})$, which is a refinement (subdivision) of $\mathcal{D}(\varphi_{\theta})$. The reconstructed polyhedral manifold has a parametric representation $\psi_{\theta} : \mathcal{F} \rightarrow \mathcal{X}$, which approximates the manifold M in the data.

Fig. 2 shows an example to demonstrate the learning results of an autoencoder. The ambient space \mathcal{X} is \mathbb{R}^3 , the manifold Σ is the buddha surface as shown in frame (a). The latent space is \mathbb{R}^2 , the encoding map $\varphi_{\theta} : \mathcal{X} \rightarrow D$ parameterizes the input manifold to a domain on $D \subset \mathcal{F}$ as shown in frame (b). The decoding map $\psi_{\theta} : D \rightarrow \mathcal{X}$ reconstructs the surface into a piecewise linear surface $\tilde{\Sigma} = \psi_{\theta} \circ \varphi_{\theta}(\Sigma)$, as shown in frame (c). In ideal situation, the composition of the encoder and decoder $\psi_{\theta} \circ \varphi_{\theta} \sim id$ should equal to the identity map, the reconstruction $\tilde{\Sigma}$ should coincide with the input Σ . In reality, the reconstruction $\tilde{\Sigma}$ is only a piecewise linear approximation of Σ .

Fig. 3 shows the cell decompositions induced by the encoding map $\mathcal{D}(\varphi_{\theta})$ and that by the reconstruction map $\mathcal{D}(\psi_{\theta} \circ \varphi_{\theta})$ for another autoencoder. It is obvious that $\mathcal{D}(\psi_{\theta} \circ \varphi_{\theta})$ subdivides $\mathcal{D}(\varphi_{\theta})$.

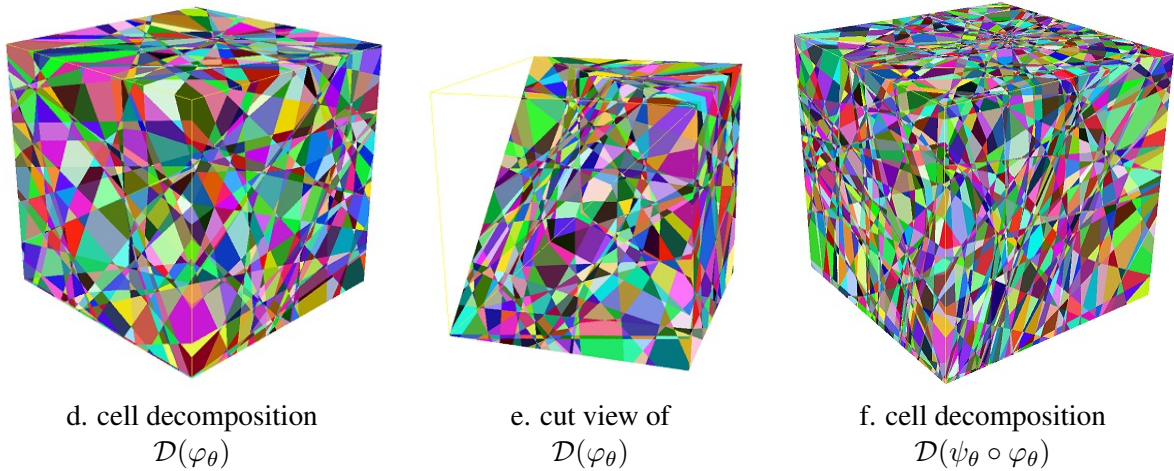


Figure 3: Cell decomposition induced by the encoding, decoding maps.

3.3 Direct Applications

Once the neural network has learned a manifold Σ , it can be utilized for many applications.

Generative Model Suppose \mathcal{X} is the space of all $n \times n$ color images, where each point represents an image. We can define a probability measure μ , which represents the probability for an image to represent a human face. The shape of a human face is determined by a finite number of genes. The facial photo is determined by the geometry of the face, the lightings, the camera parameters and so on. Therefore, it is sensible to assume all the human facial photos are concentrated around a finite dimensional manifold, we call it as human facial photo manifold Σ .

By using many real human facial photos, we can train an autoencoder to learn the human facial photo manifold. The learning process produces a decoding map $\psi_\theta : \mathcal{F} \rightarrow \tilde{\Sigma}$, namely a parametric representation of the reconstructed manifold. We randomly generate a parameter $z \in \mathcal{F}$ (white noise), $\varphi_\theta(z) \in \tilde{\Sigma}$ gives a human facial image. This can be applied as a generative model for generating human facial photos.

Denosing Tradition image denosing performs Fourier transformation of the input noisy image, then filtering out the high frequency components, inverse Fourier transformation to get the denoised image. This method is general and independent of the content of the image.

In deep learning, image denosing can be re-interpreted as geometric projection as shown in Fig. 4. Suppose we perform human facial image denosing. The clean human facial photo manifold is Σ , the noisy facial image \tilde{p} is not in Σ but close to Σ . We project \tilde{p} to Σ , the closest point to \tilde{p} on Σ is p , then p is the denoised image.

In practice, suppose an noisy facial image is given \mathbf{x} , we train an autoencoder to obtain a manifold of clean facial images represented as $\psi_\theta : \mathcal{F} \rightarrow \mathcal{X}$ and an encoding map $\varphi_\theta : \mathcal{X} \rightarrow \mathcal{F}$, then we encode the noisy image $\mathbf{z} = \varphi_\theta(\mathbf{x})$, then maps \mathbf{z} to the reconstructed manifold $\tilde{\mathbf{x}} = \psi_\theta(\mathbf{z})$. The result $\tilde{\mathbf{x}}$ is the denoised image. Fig. 5 shows the projection of several outliers onto the buddha surface using an autoencoder.

We apply this method for human facial image denosing as shown in Fig. 6, in frame (a) we project the noisy image to the human facial image manifold and obtain good denoising result; in frame (b) we use the cat facial image manifold, the results are meaningless. This shows deep learning method heavily depends on the underlying manifold, which is specific to the problem. Hence the deep learning based method is not

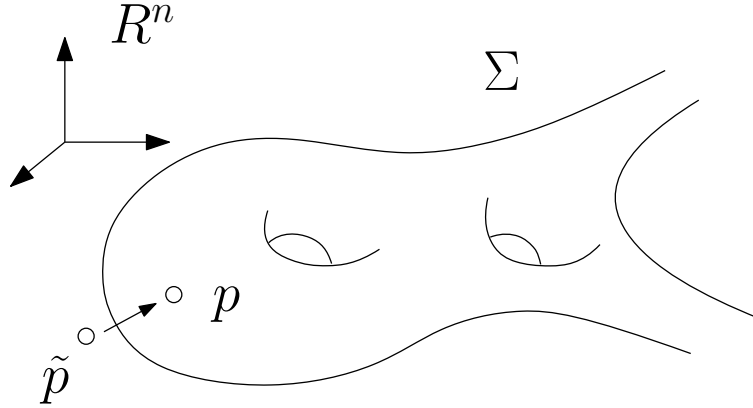


Figure 4: Geometric interpretation of image denoising.

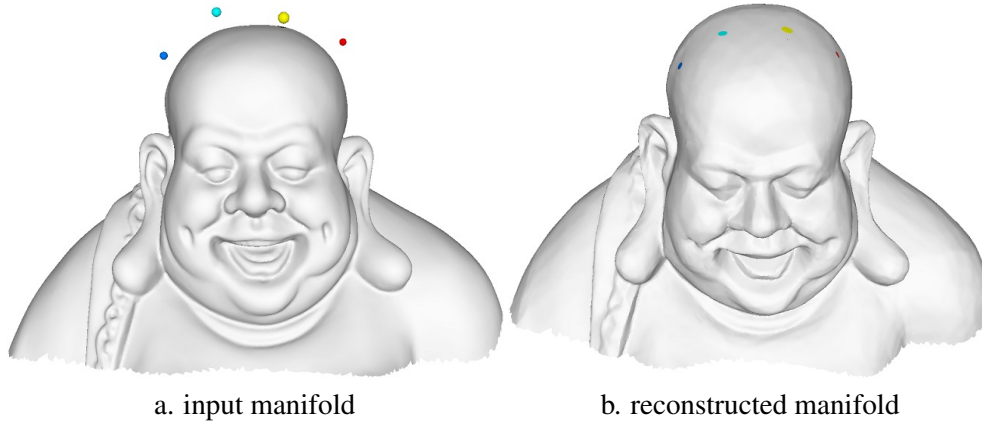


Figure 5: Geometric projection.

as universal as the conventional ones.

4 Learning Capability

4.1 Main Ideas

Fig. 7 shows another example, an Archimedean spiral curve embedded in \mathbb{R}^2 , the curve equation is given by $\rho(\theta) = (a + b\theta)e^{iw\theta}$, $a, b, w > 0$ are constants, $\theta \in (0, T]$. For relatively small range T , the encoder successfully maps it onto a straight line segment, and the decoder reconstructs a piecewise linear curve with good approximation quality. When we extend the spiral curve by enlarging T , then at some threshold, the autoencoder with the same architecture fails to encode it.

The central problems we want to answer are as follows:

1. How to decide the bound of the encoding or representation capability for an autoencoder with a fixed ReLU DNN architecture?
2. How to describe and compute the complexity of a manifold embedded in the ambient space to be encoded?

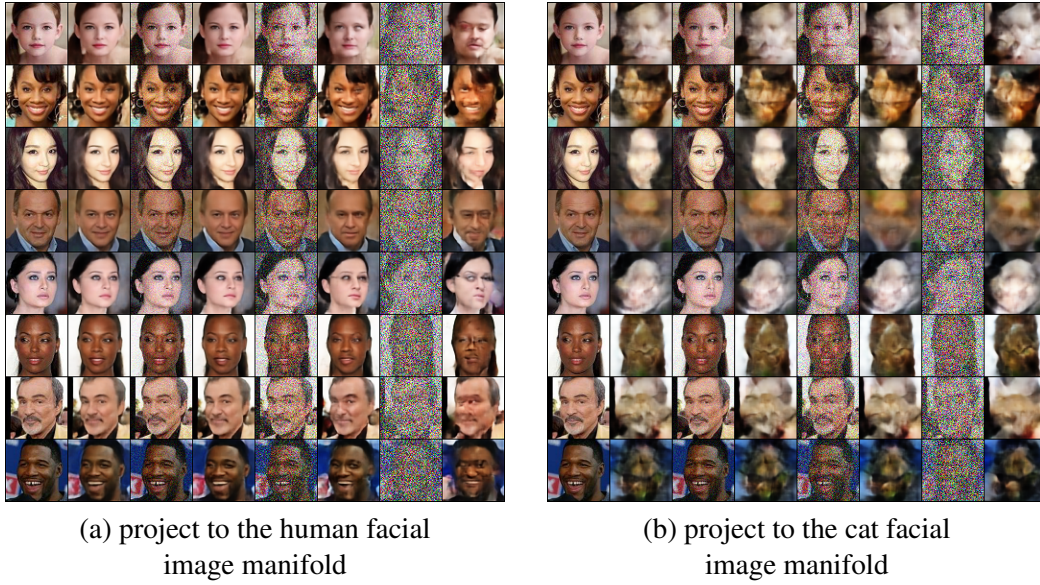


Figure 6: Image denoising.

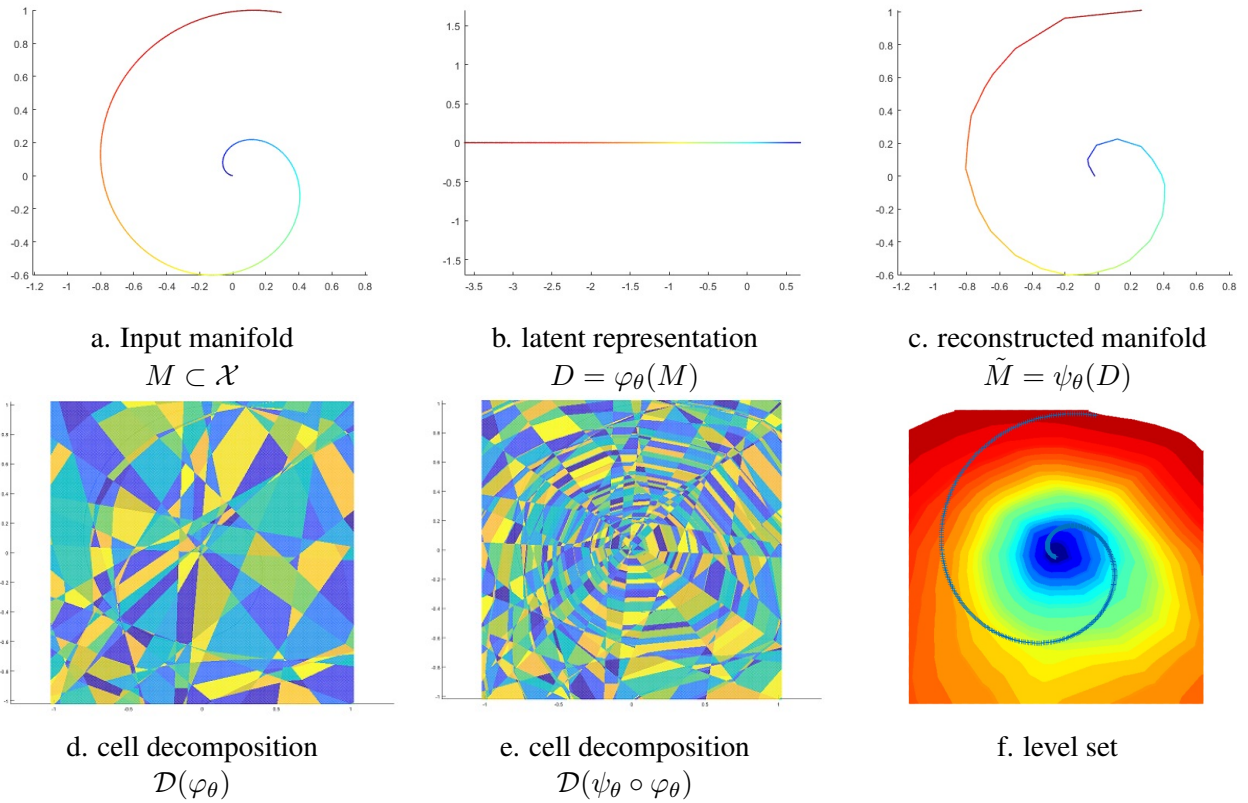


Figure 7: Encode/decode a spiral curve.

3. How to verify whether a embedded manifold can be encoded by a ReLU DNN autoencoder?

For the first problem, our solutions are based on the geometric intuition of the piecewise linear nature of encoder/decoder maps. By examining fig. 3 and fig. 7, we can see the mapping φ_θ and ψ_θ induces polyhedral cell decompositions of the ambient space \mathcal{X} , $\mathcal{D}(\varphi_\theta)$ and $\mathcal{D}(\psi_\theta \circ \varphi_\theta)$ respectively. The number of cells offers a measurement to describing the representation capabilities of these maps, the upper bound of the number of cells $\max_\theta |\mathcal{D}(\varphi_\theta)|$ describes the limit of the encoding capability of φ_θ . We call this upper bound as the *rectified linear complexity* of the autoencoder. The rectified linear complexity can be deduced from the architecture of the encoder network, as claimed in our theorem 4.5.

For the second problem, we introduce the similar concept to the embedded manifold. The encoder map φ_θ has a very strong geometric requirement: suppose U_k is a cell in $\mathcal{D}(\varphi_\theta)$, then $\varphi_\theta : U_k \rightarrow \mathcal{F}$ is an affine map to the latent space, its restriction on $U_k \cap \Sigma$ is a homeomorphism $\varphi_\theta : U_k \cap \Sigma \rightarrow \varphi_\theta(U_k \cap \Sigma)$. In order to satisfy the two stringent requirements for the encoding map: the piecewise ambient linearity and the local homeomorphism, the number of cells of the decomposition of Σ (and of \mathcal{X}) must be greater than a lower bound. Similarly, we call this lower bound the *rectified linear complexity* of the pair of the manifold and the ambient space (\mathcal{X}, Σ) . The rectified linear complexity can be derived from the geometry of Σ and its embedding in \mathcal{X} . Our theorem 4.12 gives a criteria to verify if a manifold can be rectified by a linear map.

For the third problem, we can compare the rectified linear complexity of the manifold and the autoencoder. If the RL complexity of the autoencoder is less than that of the manifold, then the autoencoder can not encode the manifold. Specifically, we show that for any autoencoder with a fixed architecture, there exists an embedded manifold, which can not be encoded by it.

4.2 ReLU Deep Neuron Networks

We extend the ReLU activation function to vectors $\mathbf{x} \in \mathbb{R}^n$ through entry-wise operation:

$$\sigma(x) = (\max\{0, x_1\}, \max\{0, x_2\}, \dots, \max\{0, x_n\}).$$

For any $(m, n) \in \mathbb{N}$, let \mathcal{A}_m^n and \mathcal{L}_m^n denote the class of affine and linear transformations from $\mathbb{R}^m \rightarrow \mathbb{R}^n$, respectively.

Definition 4.1 (ReLU DNN). *For any number of hidden layers $k \in \mathbb{N}$, input and output dimensions $w_0, w_{k+1} \in \mathbb{N}$, a $\mathbb{R}^{w_0} \rightarrow \mathbb{R}^{w_{k+1}}$ ReLU DNN is given by specifying a sequence of k natural numbers w_1, w_2, \dots, w_k representing widths of the hidden layers, a set of k affine transformations $T_i : \mathbb{R}^{w_{i-1}} \rightarrow \mathbb{R}^{w_i}$ for $i = 1, \dots, k$ and a linear transformation $T_{k+1} : \mathbb{R}^{w_k} \rightarrow \mathbb{R}^{w_{k+1}}$ corresponding to weights of hidden layers. Such a ReLU DNN is called a $(k + 1)$ -layer ReLU DNN, and is said to have k hidden layers, denoted as $N(w_0, w_1, \dots, w_k, w_{k+1})$.*

The mapping $\varphi_\theta : \mathbb{R}^{w_0} \rightarrow \mathbb{R}^{w_{k+1}}$ represented by this ReLU DNN is

$$\varphi_\theta = T_{k+1} \circ \sigma \circ T_k \circ \dots \circ T_2 \circ \sigma \circ T_1, \quad (1)$$

where \circ denotes mapping composition, θ represent all the weight and bias parameters. The depth of the ReLU DNN is $k + 1$, the width is $\max\{w_1, \dots, w_k\}$, the size $w_1 + w_2 + \dots + w_k$.

Definition 4.2 (PL Mapping). *A mapping $\varphi : \mathbb{R}^n \rightarrow \mathbb{R}^m$ is a piecewise linear mapping if there exists a finite set of polyhedra whose union is \mathbb{R}^n , and φ is affine linear over each polyhedron. The number of pieces of φ is the number of maximal connected subsets of \mathbb{R}^n over which φ is affine linear, denoted as $\mathcal{N}(\varphi)$. We call $\mathcal{N}(\varphi)$ as the rectified linear complexity of φ .*

Definition 4.3 (Rectified Linear Complexity of a ReLU DNN). *Given a ReLU DNN $N(w_0, \dots, w_{k+1})$, its rectified linear complexity is the upper bound of the rectified linear complexities of all PL functions φ_θ represented by N ,*

$$\mathcal{N}(N) := \max_\theta \mathcal{N}(\varphi_\theta).$$

Lemma 4.4. *The maximum number of parts one can get when cutting d -dimensional space \mathbb{R}^d with n hyperplanes is denoted as $\mathcal{C}(d, n)$, then*

$$\mathcal{C}(d, n) = \binom{n}{0} + \binom{n}{1} + \binom{n}{2} + \cdots + \binom{n}{d}. \quad (2)$$

Proof. Suppose n hyperplanes cut \mathbb{R}^d into $\mathcal{C}(d, n)$ cells, each cell is a convex polyhedron. The $(n + 1)$ -th hyperplane is π , then the first n hyperplanes intersection π and partition π into $\mathcal{C}(d - 1, n)$ cells, each cell on π partitions a polyhedron in \mathbb{R}^d into 2 cells, hence we get the formula

$$\mathcal{C}(d, n + 1) = \mathcal{C}(d, n) + \mathcal{C}(d - 1, n).$$

It is obvious that $\mathcal{C}(2, 1) = 2$, the formula (2) can be easily obtained by induction. □

Theorem 4.5 (Rectified Linear Complexity of a ReLU DNN). *Given a ReLU DNN $N(w_0, \dots, w_{k+1})$, representing PL mappings $\varphi_\theta : \mathbb{R}^{w_0} \rightarrow \mathbb{R}^{w_{k+1}}$ with k hidden layers of widths $\{w_i\}_{i=1}^k$, then the linear rectified complexity of N has an upper bound,*

$$\mathcal{N}(N) \leq \prod_{i=1}^{k+1} \mathcal{C}(w_{i-1}, w_i). \quad (3)$$

Proof. The i -th hidden layer computes the mapping $T_i : \mathbb{R}^{w_{i-1}} \rightarrow \mathbb{R}^{w_i}$. Each neuron represents a hyperplane in $\mathbb{R}^{w_{i-1}}$, the w_i hyperplanes partition the whole space into $\mathcal{C}(w_{i-1}, w_i)$ polyhedra.

The first layer partitions \mathbb{R}^{w_0} into at most $\mathcal{C}(w_0, w_1)$ cells; the second layer further subdivides the cell decomposition, each cell is at most subdivides into $\mathcal{C}(w_1, w_2)$ polyhedra, hence two layers partition the source space into at most $\mathcal{C}(w_0, w_1)\mathcal{C}(w_1, w_2)$. By induction, one can obtain the upper bound of $\mathcal{N}(N)$ as described by the inequality (2). □

4.3 Cell Decomposition

The PL mappings induces cell decompositions of both the ambient space \mathcal{X} and the latent space \mathcal{F} . The number of cells is closely related to the rectified linear complexity.

Fix the encoding map φ_θ , let the set of all neurons in the network is denoted as \mathcal{S} , all the subsets is denoted as $2^{\mathcal{S}}$.

Definition 4.6 (Activated Path). *Given a point $\mathbf{x} \in \mathcal{X}$, the activated path of \mathbf{x} consists all the activated neurons when $\varphi_\theta(\mathbf{x})$ is evaluated, and denoted as $\rho(\mathbf{x})$. Then the activated path defines a set-valued function $\rho : \mathcal{X} \rightarrow 2^{\mathcal{S}}$.*

Definition 4.7 (Cell Decomposition). *Fix an encoding map φ_θ represented by a ReLU RNN, two data points $\mathbf{x}_1, \mathbf{x}_2 \in \mathcal{X}$ are equivalent, denoted as $\mathbf{x}_1 \sim \mathbf{x}_2$, if they share the same activated path, $\rho(\mathbf{x}_1) = \rho(\mathbf{x}_2)$. Then each equivalence relation partitions the ambient space \mathcal{X} into cells,*

$$\mathcal{D}(\varphi_\theta) : \mathcal{X} = \bigcup_{\alpha} U_{\alpha},$$

each equivalence class corresponds to a cell: $\mathbf{x}_1, \mathbf{x}_2 \in U_{\alpha}$ if and only if $\mathbf{x}_1 \sim \mathbf{x}_2$. $\mathcal{D}(\varphi_\theta)$ is called the cell decomposition induced by the encoding map φ_θ .

Furthermore, φ_θ maps the cell decomposition in the ambient space $\mathcal{D}(\varphi_\theta)$ to a cell decomposition in the latent space. Similarly, the composition of the encoding and decoding maps also produces a cell decomposition, denoted as $\mathcal{D}(\psi_\theta \circ \varphi_\theta)$, which subdivises $\mathcal{D}(\varphi_\theta)$. Fig. 2 bottom row shows these cell decompositions.

4.4 Learning Difficulty

Definition 4.8 (Linear Rectifiable Manifold). *Suppose Σ is a m -dimensional manifold, embedded in \mathbb{R}^n , we say Σ is linear rectifiable, if there exists an affine map $\varphi : \mathbb{R}^n \rightarrow \mathbb{R}^m$, such that the restriction of φ on Σ , $\varphi|_{\Sigma} : \Sigma \rightarrow \varphi(\Sigma) \subset \mathbb{R}^m$, is homeomorphic. φ is called the corresponding rectified linear map of M .*

Definition 4.9 (Linear Rectifiable Atlas). *Suppose Σ is a m -dimensional manifold, embedded in \mathbb{R}^n , $\mathcal{A} = \{(U_{\alpha}, \varphi_{\alpha})\}$ is an atlas of M . If each chart $(U_{\alpha}, \varphi_{\alpha})$ is linear rectifiable, $\varphi_{\alpha} : U_{\alpha} \rightarrow \mathbb{R}^m$ is the rectified linear map of U_{α} , then the atlas is called a linear rectifiable atlas of Σ .*

Given a compact manifold Σ and its atlas \mathcal{A} , one can select a finite number of local charts $\tilde{\mathcal{A}} = \{(U_i, \varphi_i)\}_{i=1}^n$, $\tilde{\mathcal{A}}$ still covers Σ . The number of charts of an atlas \mathcal{A} is denoted as $|\mathcal{A}|$.

Definition 4.10 (Rectified Linear Complexity of a Manifold). *Suppose Σ is a m -dimensional manifold embedded in \mathbb{R}^n , the rectified linear complexity of Σ is denoted as $\mathcal{N}(\mathbb{R}^n, \Sigma)$ and defined as,*

$$\mathcal{N}(\mathbb{R}^n, \Sigma) := \min \{|\mathcal{A}| \mid \mathcal{A} \text{ is a linear rectifiable atlas of } \Sigma\}. \quad (4)$$

4.5 Learnable Condition

Definition 4.11 (Encoding Map). *Suppose M is a m -dimensional manifold, embedded in \mathbb{R}^n , a continuous mapping $\varphi : \mathbb{R}^n \rightarrow \mathbb{R}^m$ is called an encoding map of (\mathbb{R}^n, Σ) , if restricted on Σ , $\varphi|_{\Sigma} : \Sigma \rightarrow \varphi(\Sigma) \subset \mathbb{R}^m$ is homeomorphic.*

Theorem 4.12. *Suppose a ReLU DNN $N(w_0, \dots, w_{k+1})$ represents a PL mapping $\varphi_{\theta} : \mathbb{R}^n \rightarrow \mathbb{R}^m$, Σ is a m -dimensional manifold embedded in \mathbb{R}^n . If φ_{θ} is an encoding mapping of (\mathbb{R}^n, Σ) , then the rectified linear complexity of N is no less than the rectified linear complexity of (\mathbb{R}^n, Σ) ,*

$$\mathcal{N}(\mathbb{R}^n, \Sigma) \leq \mathcal{N}(\varphi_{\theta}) \leq \mathcal{N}(N).$$

Proof. The ReLU DNN computes the PL mapping φ_{θ} , suppose the corresponding cell decomposition of \mathbb{R}^n is

$$\mathcal{D}(\varphi_{\theta}) : \mathbb{R}^n = \bigcup_{i=1}^k U_i,$$

where each U_i is a convex polyhedron, $k \leq \mathcal{N}(\varphi_{\theta})$. If φ_{θ} is an encoding map of Σ , then

$$\mathcal{A} := \{(D_i, \varphi_{\theta}|_{D_i}) \mid D_i \cap \Sigma \neq \emptyset\}$$

form a linear rectifiable atlas of Σ . Hence from the definition of rectified linear complexity of an ReLU DNN and the manifold, we obtain

$$\mathcal{N}(\mathbb{R}^n, \Sigma) \leq \mathcal{N}(\varphi_{\theta}) \leq \mathcal{N}(N).$$

□

The encoding map $\varphi_{\theta} : \mathcal{X} \rightarrow \mathcal{F}$ is required to be homeomorphic, this adds strong topological constraints to the manifold Σ . For example, if Σ is a surface, \mathcal{F} is \mathbb{R}^2 , then Σ must be a genus zero surface with boundaries. In general, assume $\varphi_{\theta}(\Sigma)$ is a simply connected domain in $\mathcal{F} = \mathbb{R}^m$, then Σ must be a m -dimensional topological disk. The topological constraint implies that autoencoder can only learn manifolds with simple topologies, or a local chart of the whole manifold.

On the other hand, the geometry and the embedding of Σ determines the linear rectifiability of (Σ, \mathbb{R}^n) .

Lemma 4.13. Suppose a n dimensional manifold Σ is embedded in \mathbb{R}^{n+1} ,

$$M \xrightarrow{G} \mathbb{S}^n \xrightarrow{p} \mathbb{RP}^n$$

where $G : \Sigma \rightarrow \mathbb{S}^n$ is the Gauss map, \mathbb{RP}^n is the real projective space, the projection $p : \mathbb{S}^n \rightarrow \mathbb{RP}^n$ maps antipodal points to the same point, if $p \circ G(\Sigma)$ covers the whole \mathbb{RP}^n , then Σ is not linear rectifiable.

Proof. Given any unit vector $\mathbf{v} \in \mathbb{R}^{n+1}$, all the unit vectors orthogonal to \mathbf{v} form a sphere $\mathbb{S}^{n-2}(\mathbf{v})$, then $p(\mathbb{S}^{n-2}(\mathbf{v})) \cap \mathbb{RP}^n \neq \emptyset$, therefore there is a point $q \in \Sigma$, \mathbf{v} is in the tangent space at q . Line $q + t\mathbf{v}$ is tangent to Σ , by shifting the line by an infinitesimal amount, the line intersects Σ at two points. This shows there is no linear mapping, which projects Σ onto \mathbb{R}^n along \mathbf{v} . Because \mathbf{v} is arbitrary, Σ is not linear rectifiable. \square

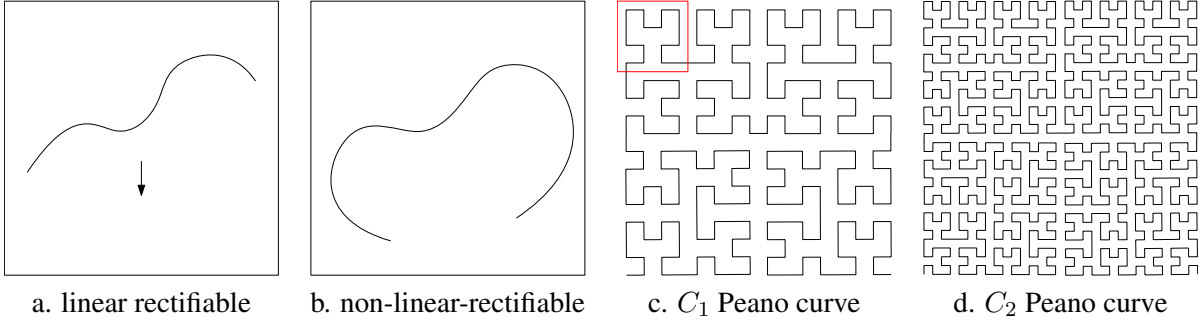


Figure 8: Linear rectifiable and non-linear-rectifiable curves.

Theorem 4.14. Given any ReLU deep neural network $N(w_0, w_1, \dots, w_k, w_{k+1})$, there is a manifold Σ embedded in \mathbb{R}^{w_0} , such that Σ can not be encoded by N .

Proof. First, we prove the simplest case. When $(w_0, w_{k+1}) = (2, 1)$, we can construct space filling Peano curves, as shown in Fig. 8. Suppose C_1 is shown in the left frame, we make 4 copies of C_1 , by translation, rotation, reconnection and scaling to construct C_2 , as shown in the right frame. Similarly, we can construct all C_k 's. The red square shows one unit, C_1 has 16 units, C_n has 4^{n+1} units. Each unit is not rectifiable, therefore

$$\mathcal{N}(\mathbb{R}^2, C_n) \geq 4^{n+1}.$$

We can choose n big enough, such that $4^{n+1} > \mathcal{N}(N)$, then C_n can not be encoded by N .

Similarly, for any w_0 and $w_{k+1} = 1$, we can construct Peano curves to fill \mathbb{R}^{w_0} , which can not be encoded by N . The Peano curve construction can be generalized to higher dimensional manifolds by direct product with unit intervals. \square

5 Control Induced Measure

In generative models, such as VAE [15] or GAN [1], the probability measure in the latent space induced by the encoding mapping $(\varphi_\theta)_*\mu$ is controlled to be simple distributions, such as Gaussian or uniform, then in the generating process, we can sample from the simple distribution in the latent space, and use the decoding map to produce a sample in the ambient space.

The buddha surface Σ is conformally mapped onto the planar unit disk $\varphi : \Sigma \rightarrow \mathbb{D}$ using the Ricci flow method [32], the uniform distribution on the parameter domain induces a non-uniform distribution on the

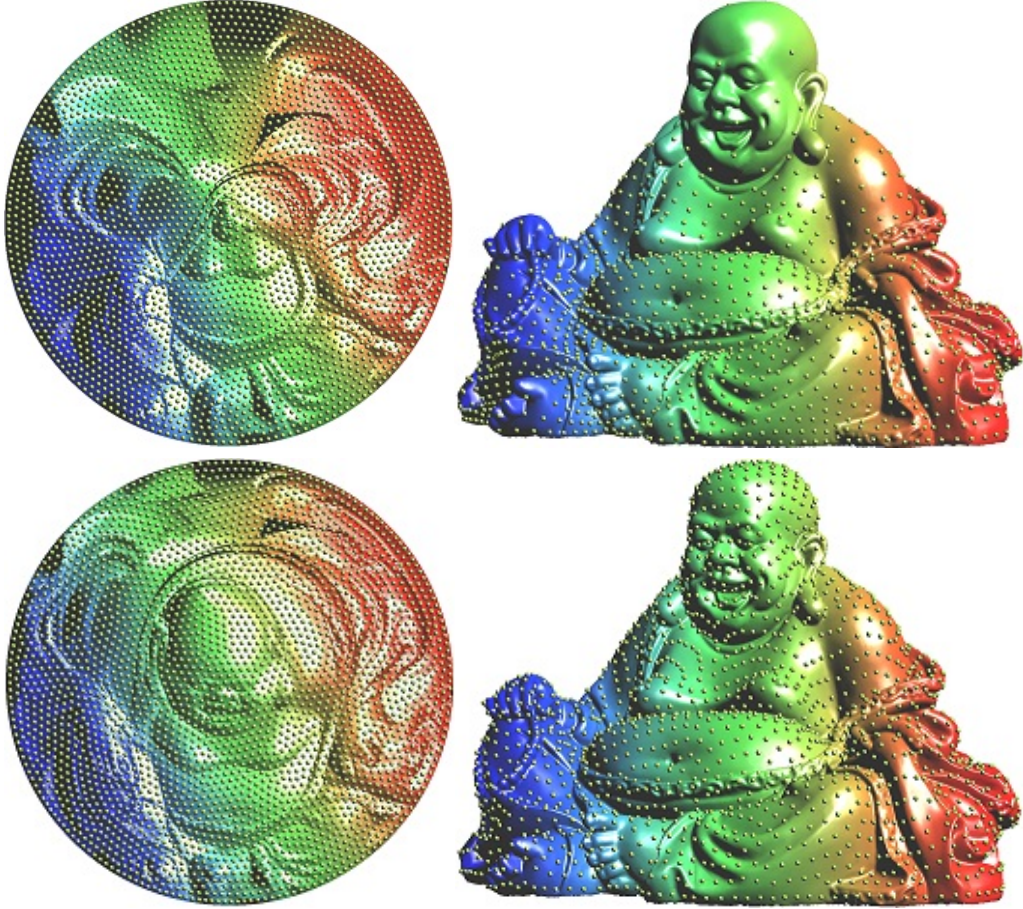


Figure 9: Control distributions by optimal mass transportation.

surface, as shown in the top row of Fig. 9. Then by composing with an optimal mass transportation map $\psi : \mathbb{D} \rightarrow \mathbb{D}$ using the algorithm in [25], one obtain an area-preserving mapping $\psi \circ \varphi : \Sigma \rightarrow \mathbb{D}$, the image is shown in the bottom row of Fig. 9 left frame. Then we uniformly sample the planar disk to get the samples $\mathbf{Z} = \{\mathbf{z}_1, \dots, \mathbf{z}_k\}$, then pull them back on to Σ by $\psi \circ \varphi$, $\mathbf{X} = \{\mathbf{x}_1, \dots, \mathbf{x}_k\}$, $x_i = (\psi \circ \varphi)^{-1}(z_i)$. Because $\psi \circ \varphi$ is area-preserving, \mathbf{Z} is uniformly distributed on the disk, \mathbf{X} is uniformly distributed on Σ as shown in the bottom row of Fig. 9 right frame.

Optimal Mass Transportation The optimal transportation theory can be found in Villani’s classical books [27][28]. Suppose $\nu = (\varphi_\theta)_*\mu$ is the induced probability in the latent space with a convex support $\Omega \subset \mathcal{F}$, ζ is the simple distribution, e.g. the uniform distribution on Ω . A mapping $T : \Omega \rightarrow \Omega$ is measure-preserving if $T_*\nu = \zeta$. Given the transportation cost between two points $c : \Omega \times \Omega \rightarrow \mathbb{R}$, the transportation cost of T is defined as

$$\mathcal{E}(T) := \int_{\Omega} c(\mathbf{x}, T(\mathbf{x})) d\nu(\mathbf{x}).$$

The *Wasserstein distance* between ν and ζ is defined as

$$\mathcal{W}(\nu, \zeta) := \inf_{T_*\nu = \zeta} \mathcal{E}(T).$$

The measure-preserving map T that minimizes the transportation cost is called the *optimal mass transportation map*.

Kantorovich proved that the Wasserstein distance can be represented as

$$\mathcal{W}(\nu, \zeta) := \max_f \int_{\Omega} f d\nu + \int_{\Omega} f^c d\zeta$$

where $f : \Omega \rightarrow \mathbb{R}$ is called the Kantorovich potential, its c-transform

$$f^c(\mathbf{y}) := \inf_{\mathbf{x} \in \Omega} c(\mathbf{x}, \mathbf{y}) - f(\mathbf{x}).$$

In WGAN, the discriminator computes the Wasserstein distance between $(\psi_{\theta})_*\zeta$ and μ . If the cost function is chosen to be the L^1 norm, $c(\mathbf{x}, \mathbf{y}) = |\mathbf{x} - \mathbf{y}|$, f is 1-Lipsitz, then $f^c = -f$, the discriminator computes the Kantorovich potential, the generator computes the optimal mass transportation map, hence WGAN can be modeled as an optimization

$$\min_{\theta} \max_f \int_{\Omega} f \circ \psi_{\theta}(\mathbf{z}) d\zeta(\mathbf{z}) - \int_{\mathcal{X}} f(x) d\mu(x).$$

The competition between the discriminator and the generator leads to the solution.

If we choose the cost function to be the L^2 norm, $c(\mathbf{x}, \mathbf{y}) = \frac{1}{2}|\mathbf{x} - \mathbf{y}|^2$, then the computation can be greatly simplified. Brenier's theorem [6] claims that there exists a convex function $u : \Omega \rightarrow \mathbb{R}$, the so-called Brenier's potential, such that its gradient map $\nabla u : \Omega \rightarrow \Omega$ gives the optimal mass transportation map. The Brenier's potential satisfies the Monge-Ampere equation

$$\det \left(\frac{\partial^2 u}{\partial x_i \partial x_j} \right) = \frac{\nu(\mathbf{x})}{\zeta(\nabla u(\mathbf{x}))}.$$

Geometrically, the Monge-Ampere equation can be understood as solving Alexandroff problem: finding a convex surface with prescribed Gaussian curvature. A practical algorithm based on variational principle can be found in [13]. The Brenier's potential and the Kantorovich's potential are related by the closed form

$$u(\mathbf{x}) = \frac{1}{2}|\mathbf{x}|^2 - f(\mathbf{x}). \tag{5}$$

Eqn.(5) shows that: the generator computes the optimal transportation map ∇u , the discriminator computes the Wasserstein distance by finding Kantorovich's potential f ; u and f can be converted to each other, hence the competition between the generator and the discriminator is unnecessary, the two deep neural networks for the generator and the discriminator are redundant.

Autoencoder-OMT model As shown in Fig. 10, we can use autoencoder to realize encoder $\varphi_{\theta} : \mathcal{X} \rightarrow \mathcal{F}$ and decoder $\psi_{\theta} : \mathcal{F} \rightarrow \mathcal{X}$, use OMT in the latent space to realize probability transformation $T : \mathcal{F} \rightarrow \mathcal{F}$, such that

$$T_*\zeta = (\varphi_{\theta})_*\mu.$$

We call this model as OMT-autoencoder.

Fig. 5 shows the experiments on the MNIST data set. The digits generated by OMT-AE have better qualities than those generated by VAE and WGAN. Fig.(5) shows the human facial images on CelebA data set. The images generated by OMT-AE look better than those produced by VAE.

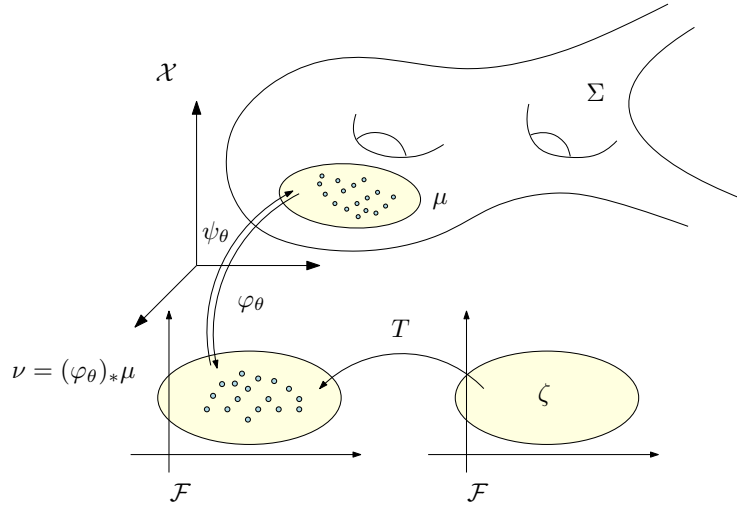
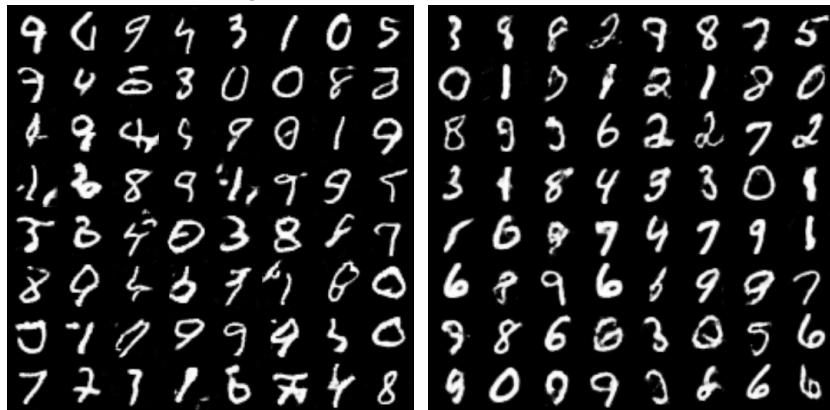


Figure 10: Autoencoder combined with a optimal transportation map.



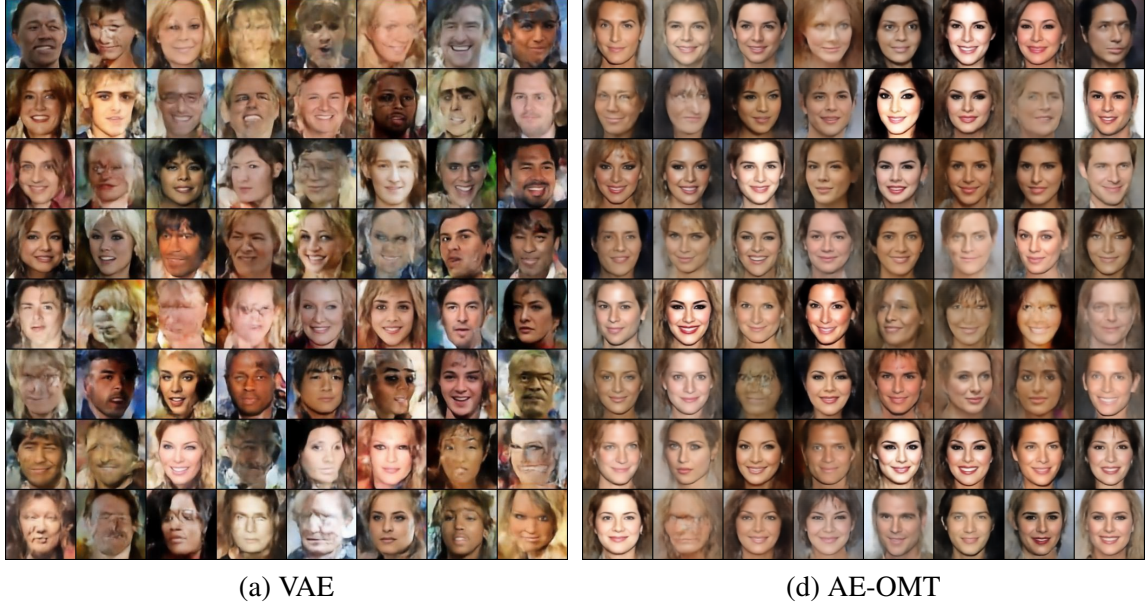
(a) real digits

(b) VAE



(c) WGAN

(d) AE-OMT



6 Conclusion

This work gives a geometric understanding of autoencoders and general deep neural networks. The underlying principle is the manifold structure hidden in data, which attributes to the great success of deep learning. The autoencoders learn the manifold structure and construct a parametric representation. The concepts of rectified linear complexities are introduced to both DNN and manifold, which describes the fundamental learning limitation of the DNN and the difficulty to be learned of the manifold. By applying the concept of complexities, it is shown that for any DNN with fixed architecture, there is a manifold too complicated to be encoded by the DNN. Experiments on surfaces show the approximation accuracy can be improved. By applying L^2 optimal mass transportation theory, the probability distribution in the latent space can be fully controlled in a more understandable and more efficient way.

In the future, we will develop refined estimates for the complexities of the deep neural networks and the embedding manifolds, generalize the geometric framework to other deep learning models.

Appendix

Here we illustrate some examples and explain the implementation details.

Facial Surface Fig. 11 shows a human facial surface Σ is encoded/decoded by an autoencoder. From the image, it can be seen that the encoding/decoding maps are homeomorphic. The Hausdorff distance between the input surface and the reconstructed surface is relatively small, but the normal deviation is big. The geometric details around the mouth area are lost during the process. There are a lot of local curvature fluctuations. Furthermore, the shape of the encoding image (parameter image) in the latent space is highly irregular, this creates difficulty for generating random samples on the reconstructed manifold.

Buddha Model Fig. 12 shows the buddha model, the top row shows the three views of the input surface, the bottom row shows the reconstructed surface. The encoder network architecture is $\{3, 768, 384, 192, 96, 48, 2\}$, the decoder network is $\{2, 48, 96, 192, 384, 768, 3\}$. The input and output spaces are \mathbb{R}^3 , the latent space is

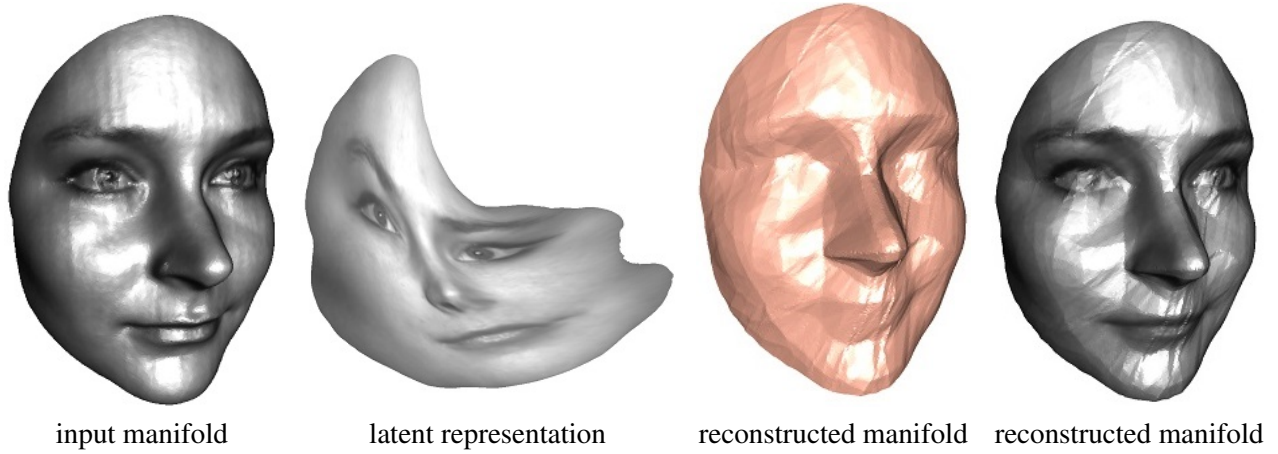


Figure 11: A human facial surface is encoded/decoded by an autoencoder.

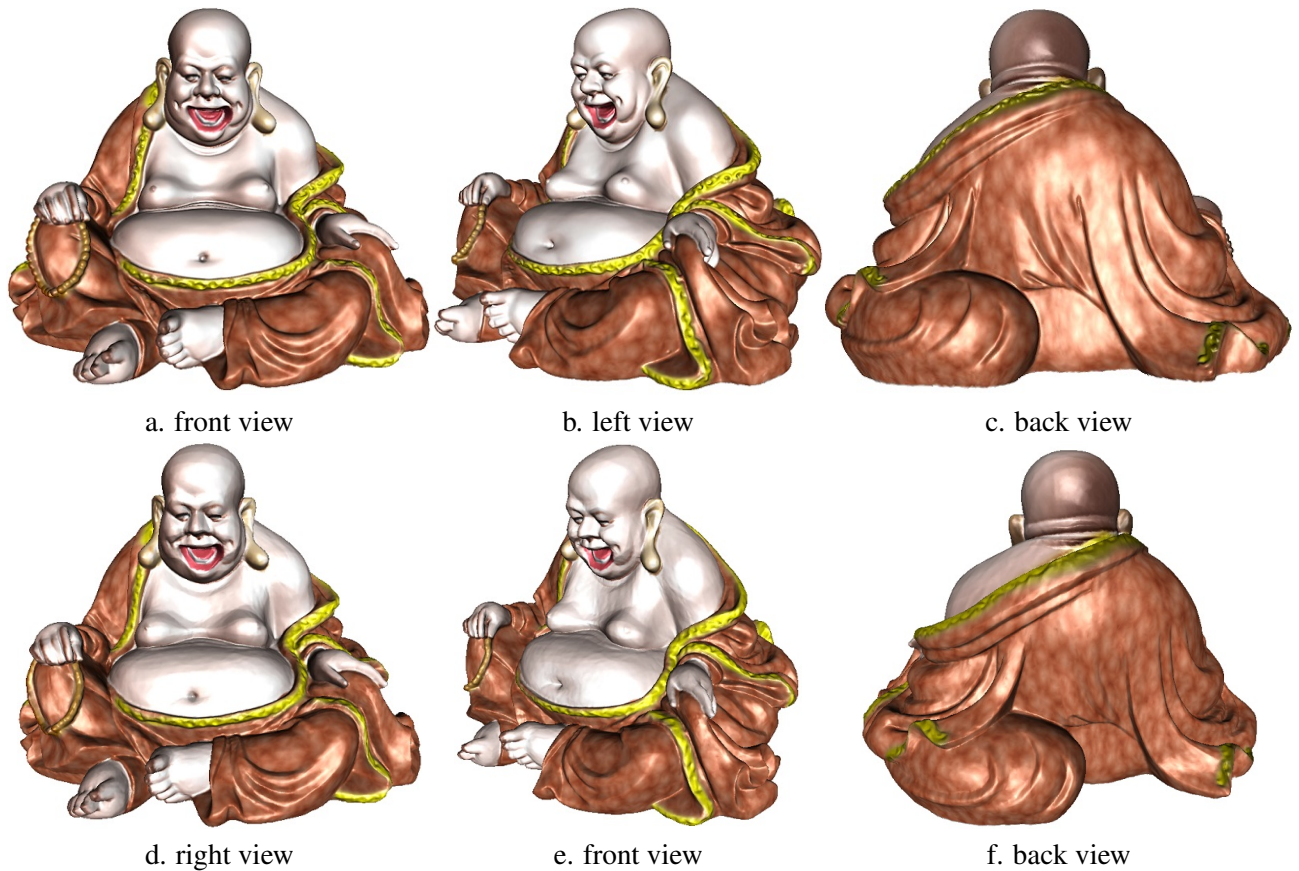


Figure 12: top row: input manifold;bottom row, reconstructed manifold.

\mathbb{R}^2 . We use ReLU as the activation function in hidden layers except the latent space layer. The loss function is the mean squared error between the input and the target. Adam optimizer is used in this autoencoder and the weight decay is set to 0 in the optimizer. From the figure, we can see the reconstruction approximates the original surface with high accuracy, all the subtle geometric features are well preserved. We uniformly

sample the surface, there are 235,771 samples in total. The number of cells in the cell decomposition induced by the reconstruction map is 230051. We see that the autoencoder produces a highly refined cell decomposition to capture all the geometric details of the input surface. The source code and the data set can be found in [34]. If we reduce the number of neurons and add regularize the output surface, then the reconstructed surface loses geometric details, and preserves the major shape as shown in Fig. 13. Furthermore, the mapping is not homeomorphic either, near the mouth and finger areas, the mapping is degenerated.

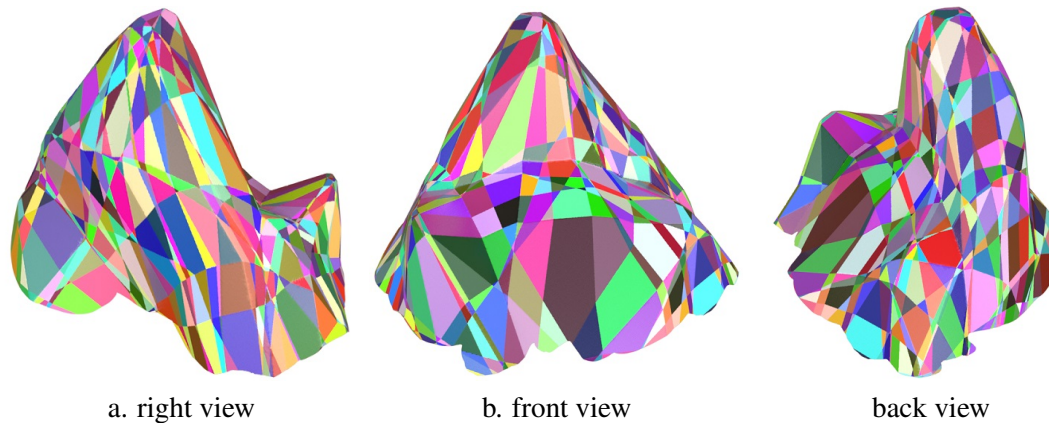


Figure 13: Reconstructed manifold with cell decomposition produced by an autoencoder with half of the neurons.

Acknowledgement

The authors thank our students: Yang Guo, Dongsheng An, Jingyao Ke, Huidong Liu for all the experimental results, also thank our collaborators: Feng Luo, Kefeng Liu, Dimitris Samaras for the helpful discussions.

References

- [1] Martin Arjovsky, Soumith Chintala, and Léon Bottou. Wasserstein generative adversarial networks. *International Conference on Machine Learning*, pages 214–223, 2017.
- [2] P. Baldi and K. Hornik. Neural networks and principal component analysis: Learning from examples without local minima. *Neural Netw.*, 2(1):53–58, January 1989.
- [3] Yoshua Bengio, Aaron Courville, and Pascal Vincent. Representation learning: A review and new perspectives. *IEEE Trans. Pattern Anal. Mach. Intell.*, 35(8):1798–1828, August 2013.
- [4] Yoshua Bengio and Yann LeCun. Scaling learning algorithms towards AI. In Leon Bottou, Olivier Chapelle, D. DeCoste, and J. Weston, editors, *Large Scale Kernel Machines*. MIT Press, 2007.
- [5] Yoshua Bengio, Li Yao, Guillaume Alain, and Pascal Vincent. Generalized denoising auto-encoders as generative models. In *Proceedings of the 26th International Conference on Neural Information Processing Systems - Volume 1*, NIPS’13, pages 899–907, USA, 2013. Curran Associates Inc.
- [6] Yann Brenier. Polar factorization and monotone rearrangement of vector-valued functions. *Comm. Pure Appl. Math.*, 44(4):375–417, 1991.
- [7] Chakravarty R. Alla Chaitanya, Anton S. Kaplanyan, Christoph Schied, Marco Salvi, Aaron Lefohn, Derek Nowrouzezahrai, and Timo Aila. Interactive reconstruction of monte carlo image sequences using a recurrent denoising autoencoder. *ACM Trans. Graph.*, 36(4):98:1–98:12, July 2017.
- [8] J. Deng, Z. Zhang, E. Marchi, and B. Schuller. Sparse autoencoder-based feature transfer learning for speech emotion recognition. In *2013 Humaine Association Conference on Affective Computing and Intelligent Interaction*, pages 511–516, Sept 2013.
- [9] X. Feng, Y. Zhang, and J. Glass. Speech feature denoising and dereverberation via deep autoencoders for noisy reverberant speech recognition. In *2014 IEEE International Conference on Acoustics, Speech and Signal Processing (ICASSP)*, pages 1759–1763, May 2014.
- [10] Peter Földiák and Malcolm P. Young. The handbook of brain theory and neural networks. chapter Sparse Coding in the Primate Cortex, pages 895–898. MIT Press, Cambridge, MA, USA, 1998.
- [11] L. Gondara. Medical image denoising using convolutional denoising autoencoders. In *2016 IEEE 16th International Conference on Data Mining Workshops (ICDMW)*, pages 241–246, Dec 2016.
- [12] Ian Goodfellow, Yoshua Bengio, and Aaron Courville. *Deep Learning*. MIT Press, 2016.
- [13] Xianfeng Gu, Feng Luo, Jian Sun, and Shing-Tung Yau. Variational principles for minkowski type problems, discrete optimal transport, and discrete monge-ampere equations. *Asian Journal of Mathematics (AJM)*, 20(2):383 C 398, 2016.
- [14] Geoffrey Hinton and Ruslan Salakhutdinov. Reducing the dimensionality of data with neural networks. *Science*, 313(5786):504 – 507, 2006.
- [15] Diederik P. Kingma and Max Welling. Auto-encoding variational bayes. *CoRR*, abs/1312.6114, 2013.
- [16] B. Lévy, S. Petitjean, N. Ray, and J. Mailliot. Least squares conformal maps for automatic texture generation. *ACM Trans. on Graphics (SIGGRAPH)*, 21(2):362–371, 2002.

- [17] Alireza Makhzani, Jonathon Shlens, Navdeep Jaitly, and Ian Goodfellow. Adversarial autoencoders. In *International Conference on Learning Representations*, 2016.
- [18] Andrew Ng. Sparse autoencoder. *CS294A Lecture Notes*, December 2011.
- [19] Bruno A. Olshausen and David J. Field. Sparse coding with an overcomplete basis set: A strategy employed by v1? *Vision Research*, 37(23):3311 – 3325, 1997.
- [20] Marc’ Aurelio Ranzato, Y-Lan Boureau, and Yann LeCun. Sparse feature learning for deep belief networks. In *Proceedings of the 20th International Conference on Neural Information Processing Systems*, NIPS’07, pages 1185–1192, USA, 2007. Curran Associates Inc.
- [21] Marc’ Aurelio Ranzato, Christopher Poultney, Sumit Chopra, and Yann LeCun. Efficient learning of sparse representations with an energy-based model. In *Proceedings of the 19th International Conference on Neural Information Processing Systems*, NIPS’06, pages 1137–1144, Cambridge, MA, USA, 2006. MIT Press.
- [22] Salah Rifai, Yoshua Bengio, Yann N. Dauphin, and Pascal Vincent. A generative process for sampling contractive auto-encoders. In *Proceedings of the 29th International Conference on International Conference on Machine Learning*, ICML’12, pages 1811–1818, USA, 2012. Omnipress.
- [23] Salah Rifai, Grégoire Mesnil, Pascal Vincent, Xavier Muller, Yoshua Bengio, Yann Dauphin, and Xavier Glorot. Higher order contractive auto-encoder. In *Proceedings of the 2011 European Conference on Machine Learning and Knowledge Discovery in Databases - Volume Part II*, ECML PKDD’11, pages 645–660, Berlin, Heidelberg, 2011. Springer-Verlag.
- [24] Salah Rifai, Pascal Vincent, Xavier Muller, Xavier Glorot, and Yoshua Bengio. Contractive auto-encoders: Explicit invariance during feature extraction. In *Proceedings of the 28th International Conference on International Conference on Machine Learning*, ICML’11, pages 833–840, USA, 2011. Omnipress.
- [25] Zhengyu Su, Yalin Wang, Rui Shi, Wei Zeng, Jian Sun, Feng Luo, and Xianfeng Gu. Optimal mass transport for shape matching and comparison. *IEEE Trans. Pattern Anal. Mach. Intell.*, 37(11):2246–2259, 2015.
- [26] C. Tao, H. Pan, Y. Li, and Z. Zou. Unsupervised spectral spatial feature learning with stacked sparse autoencoder for hyperspectral imagery classification. *IEEE Geoscience and Remote Sensing Letters*, 12(12):2438–2442, Dec 2015.
- [27] Cédric Villani. *Topics in optimal transportation*. Number 58 in Graduate Studies in Mathematics. American Mathematical Society, Providence, RI, 2003.
- [28] Cédric Villani. *Optimal transport: old and new*, volume 338. Springer Science & Business Media, 2008.
- [29] Pascal Vincent, Hugo Larochelle, Yoshua Bengio, and Pierre-Antoine Manzagol. Extracting and composing robust features with denoising autoencoders. In *Proceedings of the 25th International Conference on Machine Learning*, ICML ’08, pages 1096–1103, New York, NY, USA, 2008. ACM.
- [30] Pascal Vincent, Hugo Larochelle, Isabelle Lajoie, Yoshua Bengio, and Pierre-Antoine Manzagol. Stacked denoising autoencoders: Learning useful representations in a deep network with a local denoising criterion. *J. Mach. Learn. Res.*, 11:3371–3408, December 2010.

- [31] Jun Xu, Lei Xiang, Qingshan Liu, Hannah Gilmore, Jianzhong Wu, Jinghai Tang, and Anant Madabhushi. Stacked sparse autoencoder (ssae) for nuclei detection on breast cancer histopathology images. *IEEE Transactions on Medical Imaging*, 35(1):119–130, 1 2016.
- [32] Wei Zeng, Dimitris Samaras, and Xianfeng David Gu. Ricci flow for 3d shape analysis. *IEEE Trans. Pattern Anal. Mach. Intell.*, 32(4):662–677, 2010.
- [33] M. Zhao, D. Wang, Z. Zhang, and X. Zhang. Music removal by convolutional denoising autoencoder in speech recognition. In *2015 Asia-Pacific Signal and Information Processing Association Annual Summit and Conference (APSIPA)*, pages 338–341, Dec 2015.
- [34] https://github.com/sskqgfnnh/reconstruct_pointcloud_ae